Zonal Temperature Gradients in the Tropical Free Troposphere

Jiawei Bao,[a] Vishal Dixit,[b,c] and Steven C. Sherwood[d,e]

[a] *Max Planck Institute for Meteorology, Hamburg, Germany*
[b] *Department of Remote Sensing and Geosciences, TU Delft, Delft, Netherlands*
[c] *Interdisciplinary Programme in Climate Studies, Indian Institute of Technology Bombay, Mumbai, India*
[d] *Climate Change Research Centre, University of New South Wales, New South Wales, Sydney, Australia*
[e] *ARC Centre of Excellence for Climate Extremes, University of New South Wales, New South Wales, Sydney, Australia*

ABSTRACT: The horizontal temperature gradients in the tropical free troposphere are generally assumed to be weak. We show with ERA5 data that substantial zonal virtual temperature (T_v) gradients persist climatologically in the tropical free troposphere and investigate their causes. The gradients change seasonally: T_v at 500 hPa over the equatorial western Pacific Ocean (EWP) is usually much warmer (up to 3 K) than that over the equatorial central Pacific Ocean (ECP) during December–February (DJF), while the temperature differences between EWP and ECP are much smaller during June–August (JJA). During DJF, T_v gradients over the Pacific prevail throughout the entire free troposphere, especially in the upper troposphere near 300 hPa. We find that the associated hydrostatic pressure gradients are mainly balanced by the nonlinear terms in the momentum equation, in particular via zonal wind advection. Strong zonal winds occur near the equator in boreal winter, transporting zonal momentum so as to balance the pressure gradient force. The zonal winds are due to large-scale equatorial waves, excited by a heating pattern that is relatively symmetric about the equator. In boreal summer, the large-scale equatorial waves are less active in the Pacific region due to a more asymmetric temperature pattern, so the zonal momentum advection and T_v gradients are both much weaker. The results point to an important role of the nonlinear terms in the tropical balanced dynamics, stressing the need for an improved theoretical understanding and modeling framework of the tropical atmosphere that includes these nonlinear terms, or their net effect.

KEYWORDS: Tropics; Convection; Dynamics; Momentum

1. Introduction

The theoretical understanding of the tropical atmosphere, including both dynamics and thermodynamics, builds upon two fundamental approximations about the thermal structure of the free troposphere: first, that the temperature is nearly horizontally homogeneous on large scales (Charney 1963; Neelin and Held 1987; Bretherton and Smolarkiewicz 1989; Mapes 1993; Sobel and Bretherton 2000) and second, that the vertical temperature structure is nearly moist-adiabatic (Betts 1982; Xu and Emanuel 1989; Emanuel et al. 1994). Warm oceans near the equator frequently excite deep moist convection, which then generates gravity waves. As the Coriolis parameter is weak in the tropics, there is no force, which can readily balance the horizontal pressure gradient force in the free troposphere. With such a dynamical constraint, the fast propagating gravity waves homogenize the buoyancy as well as virtual temperature (T_v) horizontally (Bretherton and Smolarkiewicz 1989; Mapes 1993). As a result, if the virtual effect is neglected, then the whole tropics should roughly adopt a vertical thermal structure that is determined by convection—moist adiabatic.

The dynamical balance in the free troposphere is governed by the horizontal momentum equations:

$$\frac{\partial \mathbf{V}}{\partial t} + \mathbf{V} \cdot \boldsymbol{\nabla}\mathbf{V} = -\boldsymbol{\nabla}\Phi - f\mathbf{k} \times \mathbf{V}, \qquad (1)$$

where $\mathbf{V}$ is the horizontal wind vector, f is the Coriolis parameter, and Φ is geopotential. The two terms on the lhs of Eq. (1) are the partial derivative of horizontal wind with respect to time and the nonlinear advection terms while the two terms on the rhs are the pressure gradient force and Coriolis force, respectively. In the extratropics, because of the large Coriolis parameter, the main balance is between the pressure gradient force and the Coriolis force. This geostrophic balance also holds over relatively higher latitudes in the tropics, especially over 20°–30°N during boreal summer, allowing large free-tropospheric T_v gradients to develop in the Asian monsoon region when ITCZ is farther north of the equator (Wu et al. 2015).

In the deep tropics, the Coriolis parameter is very small, Eq. (1) suggests that a pressure gradient force cannot develop unless nonlinear advection terms act to balance it. The nonlinear advection terms are generally thought to be important only for short time scales—those much less than the inverse of the Coriolis parameter (Raymond 1992; Raymond et al. 2015): around 22 h at 5° and 11 h at 10° in latitude. Thereby their contributions to force balance on long time scales is often neglected. A set of equatorial waves are known to exist on time scales that can make their contributions through nonlinear terms (e.g., Kelvin–Rossby waves), although only a few studies explore dynamics of such a nonlinear balance (Van Tuyl 1986; Raymond et al. 2015). Consequently, pressure and temperature gradients are expected to be small in the tropical free troposphere (e.g., Bretherton and Smolarkiewicz 1989; Mapes 1993; Sobel and Bretherton 2000).

Corresponding author: Jiawei Bao, jiawei.bao@mpimet.mpg.de

The assumption that the temperature is homogeneous in the tropical free troposphere greatly simplifies our effort to understand the complicated tropical climate system. This has led to the idea that the essential features of the tropical atmosphere can be represented in a single column model (SCMs). SCMs have been configured in radiative–convective equilibrium (RCE) to represent the tropical atmosphere since 1960s (e.g., Manabe and Strickler 1964; Manabe and Wetherald 1967; Sarachik 1978; Nakajima et al. 1992). But such models often do not resolve large-scale dynamics. Sobel and Bretherton (2000) introduced an idealized modeling framework in which the vertical velocity can be computed based on the boundary layer temperature changes. Therefore, the vertical velocity essentially becomes a diagnostic variable. This idealized modeling framework to represent the tropical atmosphere is termed as weak temperature gradient (WTG) approximation by Sobel and Bretherton (2000). WTG has also been applied to provide large-scale conditions for idealized cloud-resolving models (CRMs) in RCE configuration over limited domains (e.g., Sessions et al. 2010; Wang and Sobel 2011; Daleu et al. 2012; Warren et al. 2020). A similar, albeit more physically motivated approach, which derives vertical velocity from momentum equations by assuming that the horizontal pressure gradient is weak in the free troposphere, is the weak pressure gradient (WPG) approximation (e.g., Kuang 2008; Blossey et al. 2009; Romps 2012; Edman and Romps 2014). Both approaches rely on the assumption that the horizontal buoyancy variations are small in the free troposphere. Although WTG was initially proposed as a specific framework for idealized modeling (Sobel and Bretherton 2000), later it has sometimes been used as a terminology to describe that the horizontal temperature structure has weak gradients, enabling a further simplification in physical interpretation. Numerous past climate studies have invoked this simplification (e.g., Pierrehumbert 1995; Miller 1997; Sherwood 1999; Emanuel 2019), and it continues to underscore findings about low cloud variability due to the implicit relationship between local SST and lower-tropospheric stability (Ceppi and Gregory 2017).

Surprisingly, very few studies have explored the horizontal temperature structure of the tropical free troposphere. The question about what limits the horizontal buoyancy and temperature gradients in the tropical free troposphere and whether they are indeed uniform remains largely unexplored. Sobel (2002) looked at the climatological January-mean fields of atmospheric temperature at 500 hPa in observations. Although he concluded that the temperature is almost uniform throughout the entire tropical belt, it should be noted that his Fig. 1 does show some zonal temperature gradients such that the midtroposphere west of 180° are about 1 K is warmer than east of it. More importantly, he only analyzed the gradients in absolute temperature, which means the virtual effect of water vapor still needs to be accounted for. Bao and Stevens (2021) compared the horizontal temperature structure from two CRM simulations with very different configurations. One simulation was from the RCEMIP project (Wing et al. 2018b), which was conducted under RCE over an elongated channel domain without rotation and SST gradient. The other one was from the DYAMOND project (Stevens et al. 2019), which applied a realistic configuration forced with observed SSTs over a global domain with rotation. They found that T_v is almost perfectly homogeneous (less than 0.5 K spatially at 500 hPa) in the RCE simulation, while the DYAMOND simulation shows more horizontal inhomogeneities especially in the upper troposphere (up to 3 K difference across the equatorial Pacific). Yang and Seidel (2020) analyzed horizontal distribution of T_v in moisture space (sorting T_v based on the corresponding column relative humidity), and showed that T_v (or equivalently buoyancy) is horizontally invariant on average within 2°N to 2°S as one goes from regions of low to high humidity using NASA AIRS data. This does not necessarily rule out systematic T_v variations but shows that they do not simply correlate with moisture (averaging T_v by moisture can help smooth out some of the spatial inhomogeneities). Zhang and Fueglistaler (2020) showed that the zonal-mean convective moist static energy in the subcloud layer is roughly constant with latitude over 20°N–20°S. With convective quasi-equilibrium approximation, this would indirectly imply that the free-tropospheric saturation moist static energy and the absolute temperature are meridionally uniform. However, they examined only meridional variations, not zonal ones.

Based on the limited results obtained from previous studies, it is unclear how uniform the horizontal temperature structure is in the tropical free troposphere and what accounts for variations. Hence, we investigate this question here. The temperature variable that we focus on is T_v. Although the horizontal differences mainly come from T, T_v is more precise as it takes into account the density effect of water vapor. The outline of the paper is as follows. Section 2 presents the data and methods. In section 3, we show substantial zonal temperature gradients exist in the tropical free troposphere. In section 4, we explain how the temperature gradients are sustained. Section 5 discusses the potential impact of such temperature gradients and section 6 summarizes the results.

2. Data and methods

ERA5 data at a horizontal resolution of 0.25° from 1979 to 2020 are used in the analysis (Hersbach et al. 2020). Most of the results are obtained with the monthly mean data. Daily data are only used when calculating horizontal momentum budgets. To better illustrate the spatial temperature structure near the equator, we plot the temperature distributions as the spatial anomalies of either annual or monthly climatological T_v. The spatial anomalies are computed by subtracting their corresponding annual/monthly climatological values averaged spatially over 20°N–20°S. Plots that display the spatial distributions include the whole tropical latitudes from 30°N to 30°S. Other type of plots focus on a narrower latitude band near the equator (8°N–8°S) where the impact of rotation is weak.

To help understand T_v gradients in the tropical free troposphere, we focus on Φ, as according to hydrostatic balance T_v and Φ are closely related:

$$\int_{p_1}^{p_2} -RT_v \, d\ln p = \int_{\Phi_1}^{\Phi_2} d\Phi, \qquad (2)$$
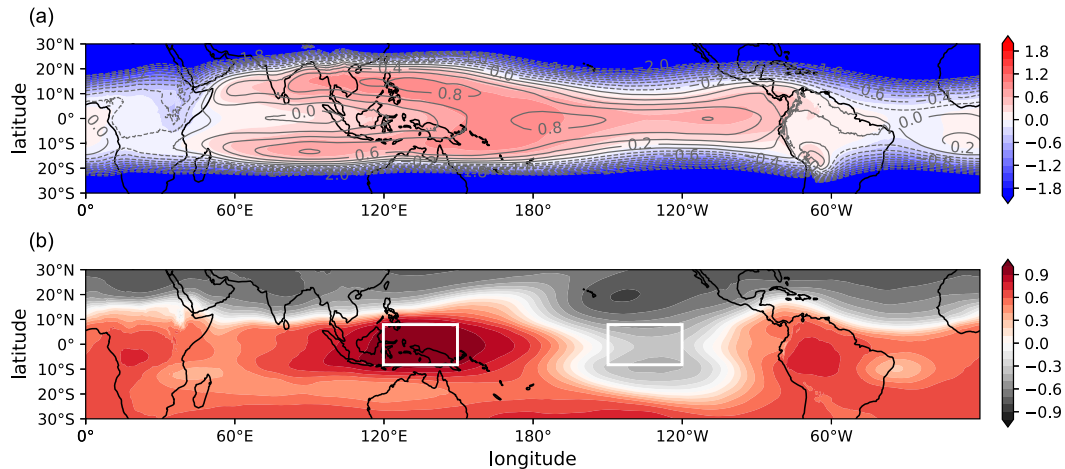
FIG. 1. (a) Spatial anomalies of the climatological annual mean T_{v500} (K; shading) and T_{500} (K; contours) averaged over 1979–2020. The spatial anomalies are computed by subtracting the spatial mean climatological T_{v500} over 20°N–20°S. (b) Spatial distributions of correlation coefficient between the spatial anomalies of the monthly mean T_{v500} over the equatorial western Pacific region (EWP) and those at every point in the tropical region. The spatial anomalies are computed by subtracting the spatial mean values over 20°N–20°S for each month. EWP (8°N–8°S, 120°–150°E) and ECP (8°N–8°S, 120°–150°W) are marked.

where p is pressure and R is the specific gas constant of dry air. We calculate the zonal momentum budget, and investigate what processes other than the Coriolis force are responsible for the balance. Here we follow Yang et al. (2013) in carrying out the analysis of zonal momentum budget. The zonal momentum equation in pressure coordinates with the nonlinear terms expanded is expressed as follows:

$$\frac{\partial \overline{u}}{\partial t} = -\frac{\partial \overline{\Phi}}{\partial x} - \left(\overline{u}\frac{\partial \overline{u}}{\partial x} + \overline{v}\frac{\partial \overline{u}}{\partial y} + \overline{\omega}\frac{\partial \overline{u}}{\partial p} \right) - \left(\frac{\partial \overline{u'u'}}{\partial x} + \frac{\partial \overline{u'v'}}{\partial y} + \frac{\partial \overline{u'\omega'}}{\partial p} \right) + f\overline{v} + X, \quad (3)$$

where u, v, and ω are the zonal velocity, meridional velocity, and vertical velocity in pressure coordinates, respectively; the overbars denote multiyear monthly means of each variable over the specific month; and primes denote daily anomalies from the multiyear monthly means. The first term on the rhs is the pressure gradient force. The second and third terms are the advection by the stationary flow and by transient eddies, respectively. The fourth term is the Coriolis force, and the last term is the residual. As we are interested in regions very close to the equator, the Coriolis force is almost negligible. Then the remaining terms should roughly balance and the residual term is expected to be small in the free troposphere except when convective momentum transports (CMT) on subdaily time scales, not included in our budget, are significant (Lin et al. 2008). We interpret all the terms that are not explicitly shown in Eq. (3) as part of the residual.

To quantify the impact of horizontal temperature gradient that may matter for energy transport in the tropical free troposphere, we look at the potential temperature equation in height coordinates:

$$\frac{\partial \theta}{\partial t} + u\frac{\partial \theta}{\partial x} + v\frac{\partial \theta}{\partial y} + w\frac{\partial \theta}{\partial z} = \frac{\theta}{c_p \rho T}Q,$$

$$\text{Adv}_h = u\frac{\partial \theta}{\partial x} + v\frac{\partial \theta}{\partial y}, \quad (4)$$

$$\text{Adv}_v = w\frac{\partial \theta}{\partial z},$$

where θ is potential temperature; T is temperature; w is vertical velocity; Q is diabatic heating; c_p is the specific heat capacity at constant pressure; ρ is air density; and Adv_h and Adv_v are horizontal and vertical temperature advection, respectively. Generally assuming a weak horizontal temperature gradient enables to neglect the horizontal temperature advection, so that the diabatic heating is balanced only by the vertical advection. We define a metric that we call advection scaling ratio: $\log_{10}(\text{Adv}_h/\text{Adv}_v)$ to compare the relative importance of horizontal versus vertical advection.

3. Observed temperature structure

We start by looking at the horizontal distribution of the virtual temperature at 500 hPa (T_{v500}) averaged over 1979–2020 (Fig. 1a). Indeed, T_{v500} is quite homogeneous especially over the Pacific Ocean near the equator as the zonal temperature difference is less than 0.3 K. The homogeneous T_{v500} pattern also extends meridionally (up to 10°–20° in latitudes in both hemispheres). We also add the contours of the absolute temperature at 500 hPa (T_{500}), and the distributions of T_{v500} and T_{500} are generally consistent, suggesting that the spatial structure in T_{v500} is mainly determined by T_{500}. The physical reasoning for such a homogeneous T_{v500} pattern is based on the assumption that the free-tropospheric temperatures near the equator are determined by regions with deep convection through gravity wave homogenization. As the most prominent
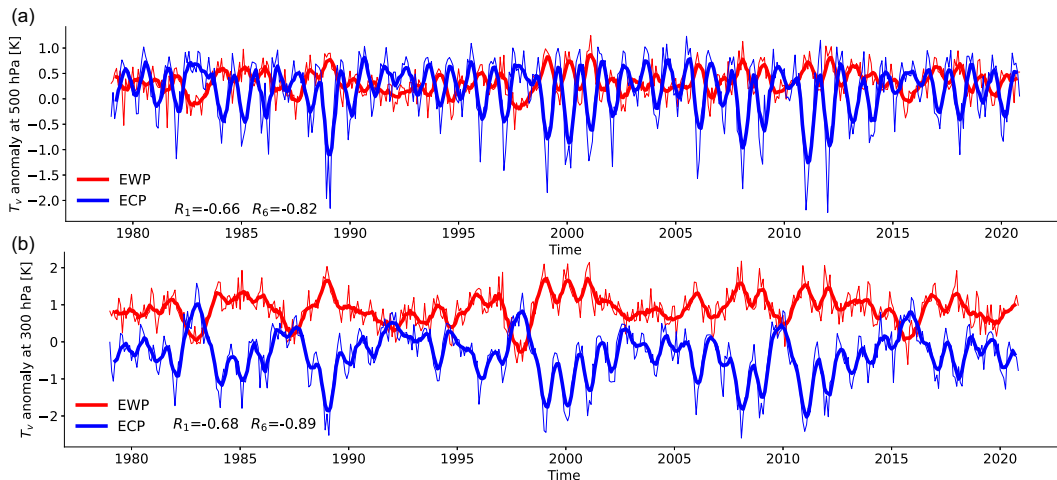
FIG. 2. Times series of the monthly mean T_v anomalies over the EWP and ECP at (a) 500 and (b) 300 hPa. Thin lines show the original data, and thick lines show the 6-month running averages. The anomalies are computed by subtracting the horizontal mean values over 8°N–8°S for each month. The Pearson correlation coefficients are calculated with the original monthly data (R_1) and 6-month running-average data (R_6).

deep convection occurs in the equatorial western Pacific Ocean (EWP), the warm sea surface temperatures there would act to regulate the temperature in the entire tropical free troposphere.

Therefore, based on the above theoretical considerations, if the tropical free-tropospheric T_v were homogeneous due to gravity wave homogenization by convection in EWP, we may expect the temporal variations in T_v throughout the tropics to follow the T_v variations in EWP. To test this assumption we look at the correlation coefficient of the time series of T_{v500} anomalies (relative to tropical means over each month) between the EWP region and each point in the tropical domain (30°N–30°S) using the monthly mean ERA5 data from 1979 to 2020 (Hersbach et al. 2020; Fig. 1b). We define EWP as regions over 8°N–8°S, 120°–150°E. Although we see strong positive correlations in most of the tropics, surprisingly, in the equatorial central and eastern Pacific Ocean there are strong negative correlations. We define these regions showing strong negative correlations as ECP (equatorial central Pacific Ocean), which are the regions over 8°N–8°S, 150°–120°W. The inconsistent temperature variations in EWP and ECP suggest that T_v must not be the same. This provides us the impetus to probe further into T_v gradients in tropical troposphere and to analyze what sustains them in the absence of Coriolis force where they do exist. Apart from the anticorrelation between T_v variations in EWP and ECP, we also note that the time series of T_v in the EWP and the Asian continent are anticorrelated (Fig. 1). This is likely related to the Asian monsoons, as the seasonal change in the monsoonal circulation can lead to such a dipole in T_v correlations between EWP and Asian continent.

Figure 2a shows the time series of the monthly mean T_{v500} anomalies in EWP and ECP. The T_{v500} anomalies in both regions show a strong seasonal cycle. When EWP has a warm T_{v500} anomaly, ECP usually has a cold T_{v500} anomaly. The monthly T_{v500} anomalies in EWP and ECP are negatively

correlated with a correlation coefficient of −0.66. The maximum T_{v500} difference between EWP and ECP can be over 3 K, which often happens during DJF, while in JJA the T_{v500} difference is slightly negative.

We perform a composite analysis by averaging the monthly T_{v500} anomalies of all Januaries, which are usually the time when T_{v500} differences are large and positive; and Julys, when T_{v500} differences are small or negative. Figure 3 illustrates that T_{v500} distributions show distinct patterns and are far from being uniform. In January, T_{v500} in EWP and Maritime Continent are warmer than the rest of the tropical domain. The relatively warm T_{v500} over EWP extends to 20° meridionally in both hemispheres. However, T_{v500} in ECP is substantially colder, even in regions close to the equator where the Coriolis force vanishes. T_{v500} over the South American Continent and neighboring eastern Pacific Oceans are also warmer than ECP. The distributions of T_{v500} roughly follows T_{500}. As water vapor is more abundant in EWP than in ECP, the virtual effect adds an extra 0.5 K on top of the absolute temperature difference. In July (northern hemispheric summer) the warmest T_{v500} regions are over the Asian Continent, far away from the equator, while over the Pacific Ocean, T_{v500} becomes more uniform. The ECP is slightly warmer than the EWP, whereas the Atlantic region is substantially cooler.

The T_v gradients are even larger in the upper troposphere. At 300 hPa, we find that T_{v300} in EWP is almost always warmer than that in ECP, and the maximum difference can be up to 4.5 K, which again usually occurs in January (Fig. 2b). Thus the above analyses indicate strong seasonal variations of the free-tropospheric T_v pattern, often with substantial horizontal gradients.

In the following, we focus on a latitude band near the equator (8°N–8°S) where the impact of rotation is very small. We first look at the vertical cross section of zonal T_v distribution in Fig. 4. In January, there are large zonal T_v differences
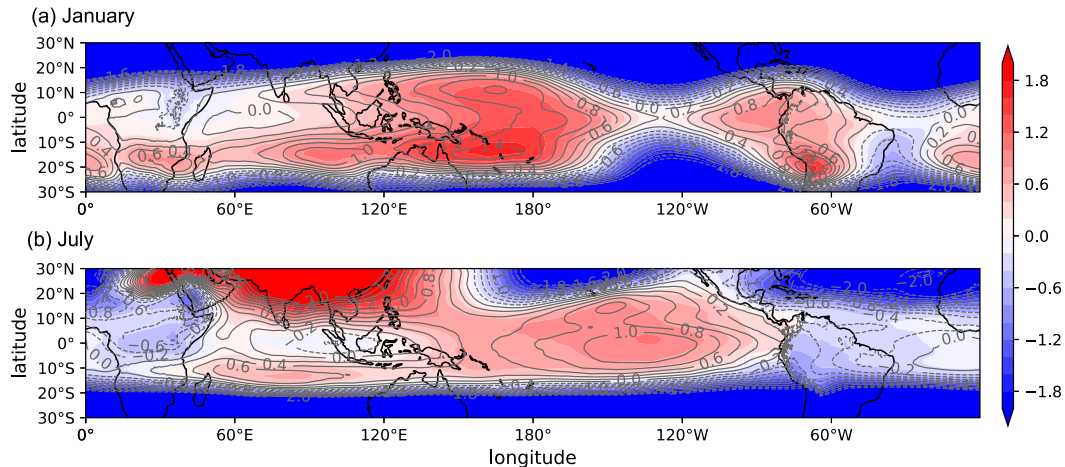
(a) January

(b) July

FIG. 3. Spatial anomalies of the climatological monthly mean T_{v500} (K; shading) and T_{500} (K; contours) averaged in (a) January and (b) July. The spatial anomalies are computed by subtracting the spatial mean values over 20°N–20°S for January and July.

throughout the entire free troposphere (Fig. 4a), consistent with Fig. 3. The upper troposphere shows especially large temperature gradients, which are almost as large as the gradients in the boundary layer where WTG is not expected to hold as turbulent friction can sustain temperature and pressure gradients.

Although such turbulent friction effects are expected to be weak in the upper troposphere, we find large T_v gradients there implying substantial pressure gradient forces. This is confirmed by analyzing the horizontal geopotential anomalies (Fig. 4c) in which the upper troposphere shows large contrasting geopotential anomalies over the west and east Pacific Ocean in January. By contrast, in July, we do not see large geopotential gradients over the Pacific Ocean. Instead, the gradients are more pronounced over the Indian Ocean, where substantial virtual temperature gradients also prevail. Note that T_v and geopotential anomalies are not collocated in their vertical distribution. This is because, according to

hydrostatic balance, it is the vertical integration of T_v between two pressure levels that determines the layer thickness. Therefore, although sometimes there are weak gradients in the geopotential field on one level, the temperature gradients can still be substantial. In such a case, the geopotential gradients may primarily manifest at levels above or below the temperature gradients.

4. How are the temperature and pressure gradients supported?

Since gradients in pressure/geopotential have to be balanced in the momentum equation, we calculate the zonal momentum budget, and investigate what processes other than the Coriolis force are responsible for the balance. Each budget is calculated for January and July (Fig. 5). In both months, the zonal momentum budget is almost closed in the free troposphere as the residual terms are small, suggesting that the

(a) January   (c) January
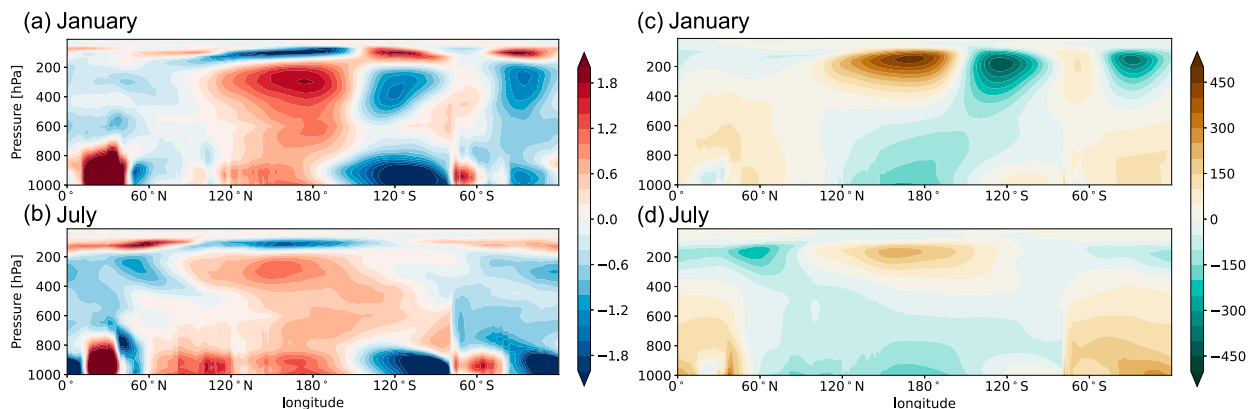

(b) July   (d) July

FIG. 4. (a),(b) Mean virtual temperature anomalies (K) and (c),(d) mean geopotential height anomalies (m) on the longitude–pressure cross section averaged between 8°N and 8°S. The anomalies are calculated relative to the mean over each pressure level. (a),(c) January and (b),(d) July.
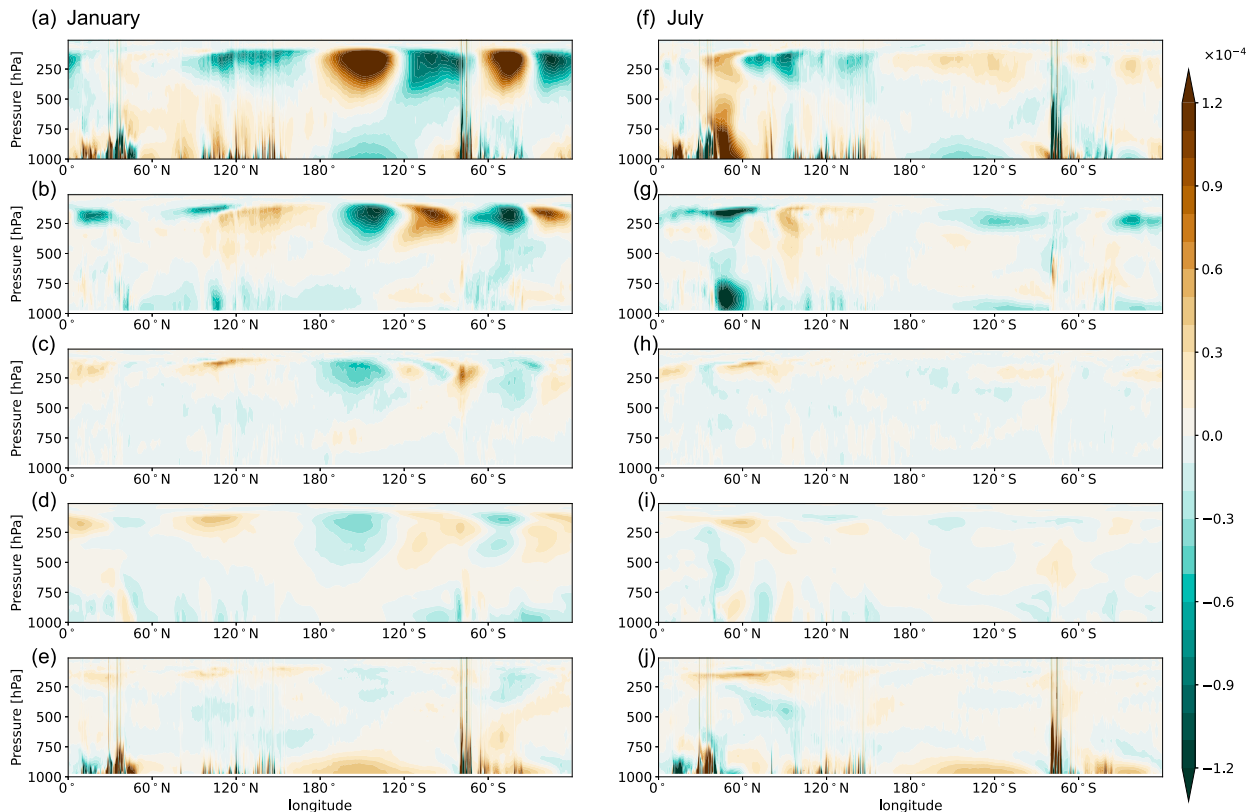
FIG. 5. Mean zonal momentum budget on the longitude–pressure cross section averaged between 8°N and 8°S. (a),(f) Pressure gradient force; (b),(g) advection by stationary flows; (c),(h) advection by transient eddies; (d),(i) Coriolis force; and (e),(j) the residual. Units are m s^{-2}. (a)–(e) January and (f)–(j) July.

contributions from subdaily CMT are not large when averaged over the month. In the boundary layer, however, the residual terms are much larger especially over land, signifying the important role of surface friction (or shallow CMT) in the zonal momentum balance (Lin et al. 2008; Helfer et al. 2021). Note that over some land points, large magnitude of pressure gradient force (therefore residuals) also extends throughout the entire vertical column. This could be due to numerical issues. In January the main balance is between the pressure gradient force (Fig. 5a) and the advection by stationary flow [second term on rhs of Eq. (3), Fig. 5b]. This balance prevail in both the Pacific and Atlantic regions where pressure gradient forces are relatively large. The advection by transient eddies and Coriolis force also contribute to the balance, but are much weaker. The same dominant balance occurs in July, but with smaller gradients.

We further probe the mean advection term by decomposing it into mean zonal, meridional, and vertical advective components. We find that the dominant component at all levels where substantial zonal geopotential/pressure gradients were noted before (Fig. 6), is the zonal advection component. This is consistent with Yang et al. (2013) who calculated the budget of zonal momentum equations with ERA-Interim data. Therefore, the strong zonal pressure gradient force is primarily sustained by the mean zonal wind advection, $-\overline{u}\,\partial\overline{u}/\partial x$.

We next analyze the spatial patterns of the wind field to understand the accelerations due to mean wind (Fig. 7). The wind field in the upper troposphere shows that the westerlies near the equator are very strong and accelerate in ECP, thus appearing in the budget as zonal wind advection enabling the mean zonal wind advection. Then the logical question to ask is what drives strong westerlies here? One possibility is that these winds are simply a part of the upper branch of the Walker Circulation as it flows from west to east. To test this we apply the Helmholtz decomposition (e.g., Hawkins and Rosenthal 1965; Sangster 1987) using the windspharm Python package (Dawson 2016) and divide the zonal wind field into a divergent component (u_d) and a rotational component (u_r):

$$u = u_d + u_r. \tag{5}$$

The Walker Circulation is an overturning circulation whose strength can be measured via the zonal streamfunction using only the divergent wind component (Schwendike et al. 2014), since the rotational wind that is nondivergent does not contribute to it. Following this we can rule out the possibility that the strong westerlies in the upper troposphere are a part of the Walker Circulation, as we find that the zonal winds near the equator in ECP are mainly dominated by the rotational component, while the divergent component
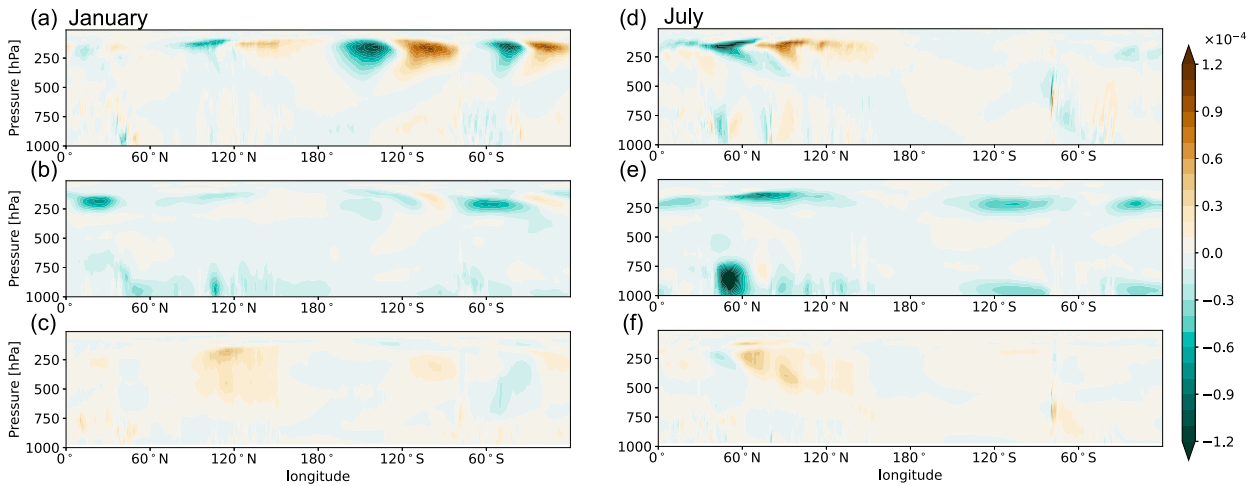
FIG. 6. Mean zonal momentum budget decomposed into advection by (a),(d) zonal wind; (b),(e) meridional wind; and (c),(f) vertical wind on the longitude–pressure cross section averaged between 8°N and 8°S. Units are m s^{-2}. (a)–(c) January and (d)–(f) July.

associated with the Walker circulation is an order of magnitude weaker (Fig. 8).

The rotational wind is often linked to tropical wave activity (Sardeshmukh and Hoskins 1988; Yasunaga and Mapes 2012). We find (Fig. 7) that the circulation pattern in January broadly resembles the planetary wave response to an isolated equatorial mass or midtropospheric heat source symmetric about the equator on an equatorial β plane, with a Kelvin-wave-like structure to the east of the source and Rossby waves to the west (Gill 1980). This may suggest that the key circulation is a classic, damped linear wave response to convective heating. However, there are important differences between the observed pattern and the Gill solution. The observed pattern is significantly broader in horizontal extent and is asymmetric about the equator. A probable reason is that, although the strongest

convection mainly occurs near the equator in EWP, the average location is a little bit south of the equator as the Australian monsoon is active in January. As a consequence, the heating pattern is not exactly symmetric. More importantly, in reanalysis data nonlinearities related to momentum advection are retained and were found above to be crucial, but they are neglected in the linear damped solutions. We therefore find that the observed equatorial waves on one hand resemble in its spatial pattern the linear Kelvin and Rossby wave solutions, but on the other hand involve a significant zonal pressure gradient force that is not captured in the linear solutions to the shallow water equations. Indeed, Lin et al. (2008) found that a strong damping is needed in the Gill model because nonlinear advection contributes to balance the pressure gradient force, but the
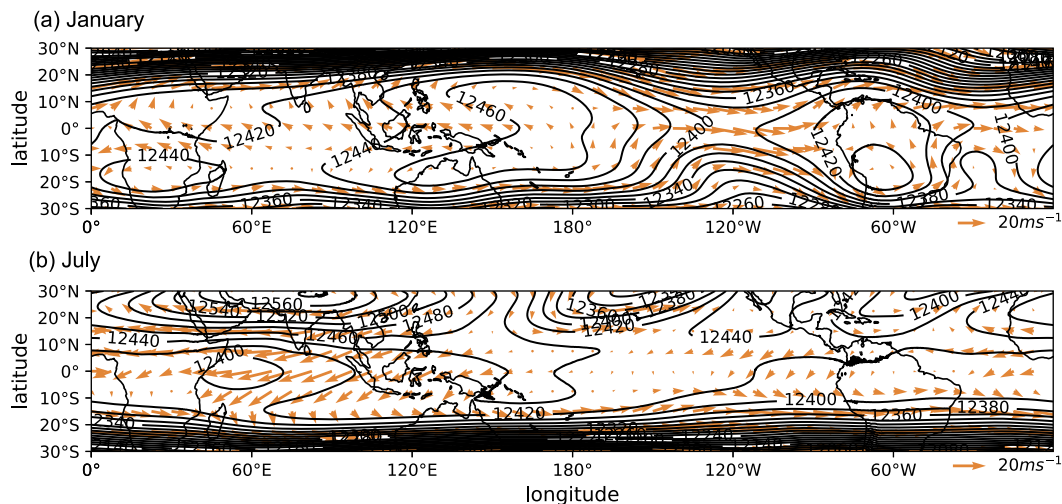

FIG. 7. Spatial distributions of the climatological monthly mean wind (vectors; m s^{-2}) and geopotential height (contours; m) at 200 hPa in (a) January and (b) July.

(a) January rotational component
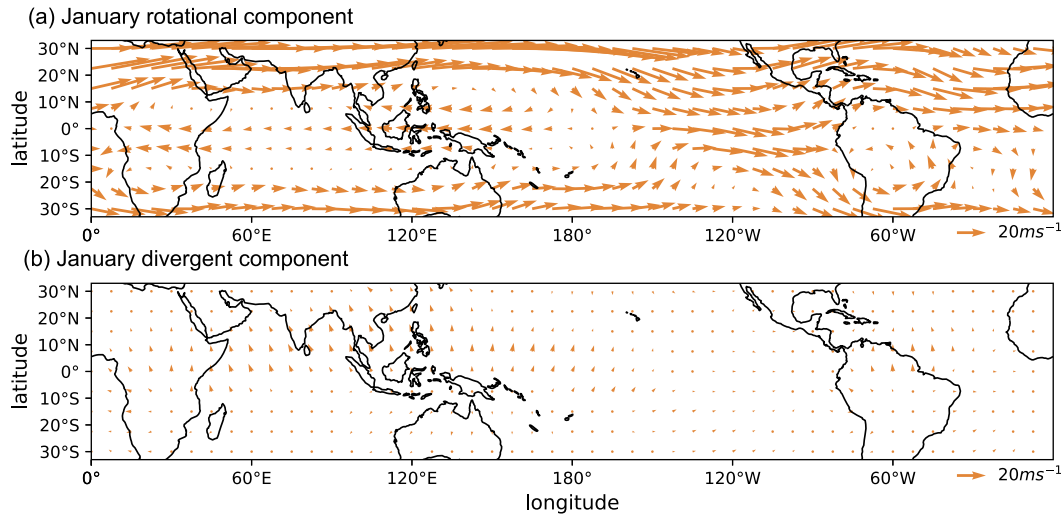

(b) January divergent component

FIG. 8. Spatial distributions of the climatological monthly mean wind decomposed into (a) rotational component and (b) divergent component at 200 hPa in January.

damping rate is spatially inhomogeneous. Van Tuyl (1986) compared nonlinear and linear solutions of the shallow water model for idealized tropical heating (mass sink), finding that when this is latitudinally symmetric (corresponding to convective heating), the zonal wind near the equator is stronger in the nonlinear solution. Dima et al. (2005) showed that many characteristics of the circulation pattern can be replicated by the nonlinear solution to the shallow water equations with a heat source centered 8° south of the equator.

In July, when the gradients are relatively small, all terms are small over the Pacific regions (Figs. 5f–j), because there is no strong zonal wind to sustain pressure or temperature gradients. Indeed during the boreal summer the strong convective heating occurs over the Asian continent, far away from the equator, and the wave activity and winds are weak near the equator. As a result the winds over the Pacific are weak and the temperature gradients are small (Fig. 7). Meanwhile, we see strong zonal winds over the Indian Ocean, where the mean advection is again contributed mainly by zonal component associated with the monsoonal circulation (Fig. 6d). These winds explain the pressure gradients and temperature gradients there.

Finally, we show the relationship between horizontal T_v structure and the upper-tropospheric zonal wind in Fig. 9. As expected, the T_v difference and regional zonal wind are highly correlated, with $R = 0.85$. Positive temperature gradients between EWP and ECP occur during westerly winds, negative gradients occur during easterlies, and uniform T_v structure occurs when the zonal wind speed is close to zero. This again confirms that substantial horizontal temperature gradients do exist in the tropical free troposphere, and are mainly maintained by the strong zonal winds near the equator, which in turn are driven by the rotational winds associated with nonlinear equatorial waves.

The seasonal contrast in the temperature gradients over the equatorial Pacific suggests that WTG approximation is

followed more closely only during boreal summer while its applicability during boreal winter depends on the importance of nonlinear terms. Although the gravity wave homogenization of the free-tropospheric temperature is not always the main restoring mechanism, lessons can still be learned for WTG from the relationships between the horizontal T_v anomalies and vertical temperature advection. One possibility to incorporate this seasonal contrast into the current WTG framework is to take into consideration the relative difference in the time scale of WTG establishment and the time scale of the phenomenon under investigation. One may apply different relaxation time scales for WTG implementation during different seasons, with larger (shorter) relaxation time scales during boreal winter (summer). The relaxation time scales can be roughly estimated by regressing virtual temperature anomalies against vertical temperature advection. Figure 10 shows that the relaxation time scales are generally shorter in July than in January and depend on height. If we assume that damping is
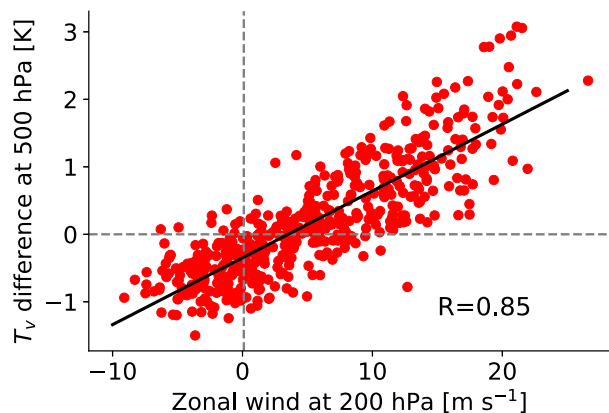

FIG. 9. Scatterplot of monthly mean zonal wind averaged over the central and eastern Pacific region (8°N–8°S, 180°–80°W) at 200 hPa vs T_v difference between EWP and ECP at 500 hPa.
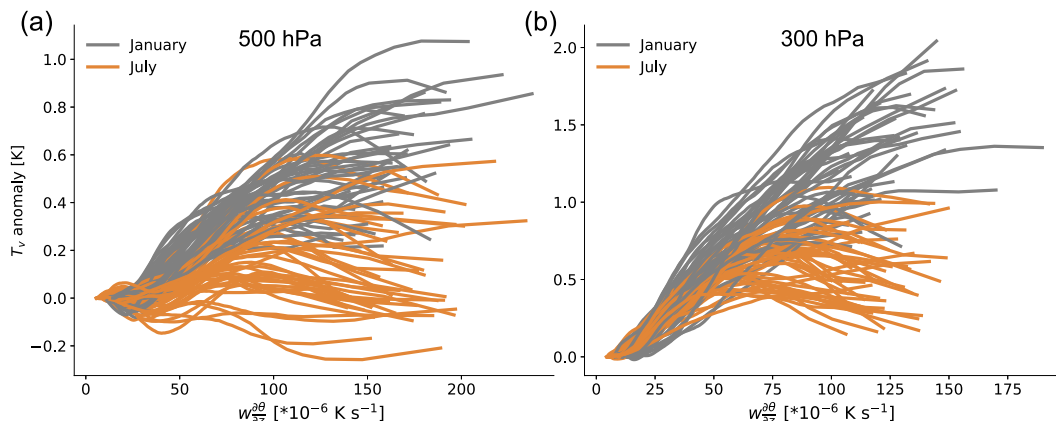
FIG. 10. T_v anomalies over the deep tropical latitude regions (8°N–8°S) as a function of vertical temperature advection [$w\partial\theta/\partial z$] calculated for (a) 500 and (b) 300 hPa. T_v anomalies are sorted by $w\partial\theta/\partial z$ and plotted as a function of $w\partial\theta/\partial z$ percentiles. Monthly mean data over 1979–2020 are used, and each line represents the relationship between T_v anomalies and $w\partial\theta/\partial z$ in either January or July.

linear, then in January the relaxation time scales are between 1 and 2 h at 500 hPa, whereas they are about 4 h at 300 hPa.

5. Discussion

We have shown that substantial zonal temperature gradients exist in the tropical free troposphere. Then the question is: what gradient can be considered as weak? We compare the relationship between spatial T_v difference (relative to T_v at EWP) and advection scaling ratio $\log_{10}(\mathrm{Adv}_h/\mathrm{Adv}_v)$ in Fig. 11. When $\log_{10}(\mathrm{Adv}_h/\mathrm{Adv}_v) = -1$, vertical advection is an order of magnitude larger than horizontal advection. This roughly corresponds to a temperature difference of about 2 K. Above
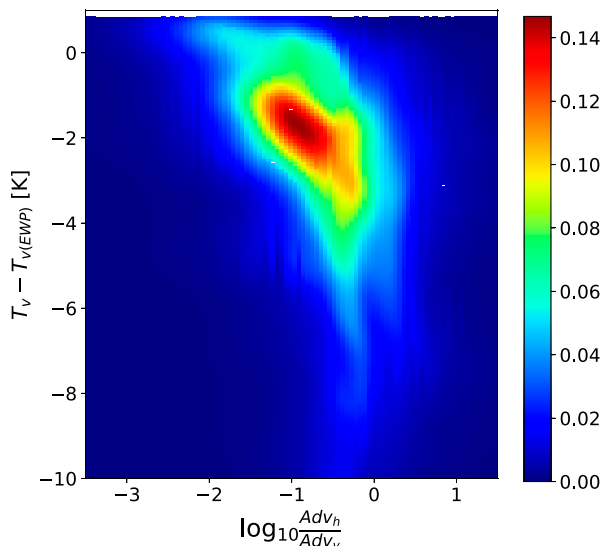

FIG. 11. Kernel density estimation of the probability distribution function of the climatological monthly mean advection scaling ratio $\log_{10}(\mathrm{Adv}_h/\mathrm{Adv}_v)$ and spatial T_v difference (K; relative to T_v over EWP) at 300 hPa over 30°N–30°S in January.

that, horizontal advection becomes increasingly important and may be not neglected. Thus, when T_v in some non-convective tropical regions is colder than T_v in EWP by over 2 K, horizontal advection also acts to balance a nonnegligible part of the diabatic heating.

Although horizontal advection helps to balance the diabatic heating (mainly radiative cooling in some of the non-convective regions), modeling the regional atmosphere in the tropics by applying the WTG framework in an idealized SCM or CRM may still be valid. Because the convective heating resulted from temperature difference relative to the target temperature in the convective regions as described in WTG is several orders of magnitude larger than the horizontal advection. In the end, it is still mainly the vertical advection that acts to balance the convective heating. Our results confirm, however, that the background temperature in the upper troposphere in some non-convective regions should actually be a couple of degrees cooler than the tropical mean temperature.

An inhomogeneous horizontal temperature structure has potentially important impacts, particularly, thermodynamic effects on the tropospheric stability. Convection takes place in a less stable condition than the environment assuming a uniform horizontal temperature. This may explain why convection is sometimes too organized in RCE simulations (Wing et al. 2018a; Holloway et al. 2017), because the free-tropospheric virtual temperature distribution is almost perfectly uniform, leading to a too-stable condition where the convection is happening. Additionally, convective available potential energy (CAPE) is sensitive to the environment temperature. Several degrees colder in the environment temperature could lead to a substantial increase in CAPE.

The results here can also help explain why the vertical thermal structure in the tropical free troposphere is not exactly moist-adiabatic relative to ascending parcels in convective regions. Some previous studies attribute departures from moist-adiabats to the impact of entrainment, as most of the rising saturated air parcels mix with the nonsaturated environment

during ascent (Singh and O'Gorman 2013, 2015; Zhou and Xie 2019; Bao et al. 2021; Keil et al. 2021). This argument essentially accepts a homogeneous horizontal temperature structure and assumes that deep convective parcels determine the thermal structure everywhere in the tropics, while attributing the departures from the moist-adiabatic structure solely to the entrainment. Our result suggests that the inhomogeneous horizontal temperature distribution could also push the tropical mean vertical structure away from a moist adiabat because of spatial averaging between convective (warm) and non-convective (cool) regions, even if convection locally enforces such an adiabat. In particular, this explains why the temperature structure often deviates from a moist adiabat in the upper troposphere across all the DYAMOND models (Bao and Stevens 2021).

From the perspective of dynamics, a warmer free troposphere in the deep convective regions contributes to the low surface pressure, which would enhance the mass convergence and circulation. This suggests that we cannot rely solely on boundary layer temperature patterns to predict the surface pressure gradient and circulation. This may explain why Lindzen and Nigam (1987) had to extend the height of the boundary layer to 700 hPa in their calculations to obtain a realistic flow field with no geopotential gradient at the PBL top. The contributions from above 700 hPa can also be important, as shown here.

6. Conclusions

In this study we report substantial zonal virtual temperature gradients in the free troposphere near the equator in contrast to conventional wisdom. The virtual temperature at 500 hPa over the equatorial western Pacific Ocean (EWP) can sometimes be up to 3 K warmer than that over the equatorial central Pacific Ocean (ECP). These zonal temperature gradients show strong seasonal variations: they mainly occur in boreal winter when the free-tropospheric temperature over EWP is substantially warmer than that over ECP. Meanwhile, the virtual temperature gradient pattern (warmer over EWP, colder over ECP) exists consistently throughout the entire free troposphere, and is most pronounced in the upper troposphere near 300 hPa where the virtual temperature difference between EWP and ECP can be as large as 4.5 K. In boreal summer, the virtual temperature over the Pacific Ocean becomes more homogeneous.

The large virtual temperature gradients in the upper troposphere indicate strong pressure gradient forces. This is in contrast to many previous studies, arguing that such gradients cannot develop in the free troposphere near the equator because the Coriolis force is too weak (Bretherton and Smolarkiewicz 1989; Sobel and Bretherton 2000) or finding them to be absent in models with idealized geometries (Bao and Stevens 2021). We find that although the Coriolis force is very weak near the equator, the pressure gradient force there is balanced by steady zonal momentum advection associated with strong zonal winds. Furthermore, by decomposing the winds into divergent and rotational components, we find that the strong zonal winds during the

boreal winter are mainly rotational and are related to nonlinear large-scale equatorial waves. The nature of large-scale equatorial waves are strongly linked to the pattern of convective heating. When the major heating due to active convection occurs closer to the equator, such as in boreal winter, the equatorial waves are very active. Whereas in boreal summer, as the strong convection takes place in the Asian Continent, which is far away from the equator, the large-scale equatorial waves become less active in the Pacific region, and therefore the zonal winds become too weak to sustain free-tropospheric pressure or temperature gradients near the equator. Meanwhile, strong zonal winds associated with the monsoonal circulation develop in the Indian Ocean region, resulting in substantial temperature gradients there in the upper troposphere.

An inhomogeneous temperature structure in the tropical free troposphere have important thermodynamic impacts on the tropospheric stability, and dynamical impacts on the surface pressure. Additionally, it also suggests that horizontal temperature advection should not always be neglected. We find that horizontal and vertical temperature advections are equally important in some non-convective tropical regions when the virtual temperature there is over 2 K colder than in the deep convective regions.

This study highlights the important role of the nonlinear advection term in the dynamical balance equations over the tropical free troposphere where the impact of Coriolis force is very weak. It agrees with Raymond et al. (2015) who pointed out that balanced dynamics, mainly the nonlinear dynamics, and convection work together in the tropics, emphasizing the need to account for the nonlinear terms in the theoretical understanding of the tropical atmosphere.

REFERENCES

Bao, J., and B. Stevens, 2021: The elements of the thermodynamic structure of the tropical atmosphere. *J. Meteor. Soc. Japan*, **99**, 1483–1499, https://doi.org/10.2151/jmsj.2021-072.

——, ——, L. Kluft, and D. Jiménez-de-la Cuesta, 2021: Changes in the tropical lapse rate due to entrainment and their impact on climate sensitivity. *Geophys. Res. Lett.*, **48**, e2021GL094969, https://doi.org/10.1029/2021GL094969.

Betts, A. K., 1982: Saturation point analysis of moist convective overturning. *J. Atmos. Sci.*, **39**, 1484–1505, https://doi.org/10.1175/1520-0469(1982)039<1484:SPAOMC>2.0.CO;2.

Blossey, P. N., C. S. Bretherton, and M. C. Wyant, 2009: Subtropical low cloud response to a warmer climate in a superparameterized climate model. Part II: Column modeling with a

cloud resolving model. *J. Adv. Model. Earth Syst.*, **1** (3), https://doi.org/10.3894/JAMES.2009.1.8.

Bretherton, C. S., and P. K. Smolarkiewicz, 1989: Gravity waves, compensating subsidence, and detrainment around cumulus clouds. *J. Atmos. Sci.*, **46**, 740–759, https://doi.org/10.1175/1520-0469(1989)046<0740:GWCSAD>2.0.CO;2.

Ceppi, P., and J. M. Gregory, 2017: Relationship of tropospheric stability to climate sensitivity and Earth's observed radiation budget. *Proc. Natl. Acad. Sci. USA*, **114**, 13 126–13 131, https://doi.org/10.1073/pnas.1714308114.

Charney, J. G., 1963: A note on large-scale motions in the tropics. *J. Atmos. Sci.*, **20**, 607–609, https://doi.org/10.1175/1520-0469(1963)020<0607:ANOLSM>2.0.CO;2.

Daleu, C. L., S. J. Woolnough, and R. S. Plant, 2012: Cloud-resolving model simulations with one- and two-way couplings via the weak temperature gradient approximation. *J. Atmos. Sci.*, **69**, 3683–3699, https://doi.org/10.1175/JAS-D-12-058.1.

Dawson, A., 2016: Windspharm: A high-level library for global wind field computations using spherical harmonics. *J. Open Res. Software*, **4**, e13, https://doi.org/10.5334/jors.129.

Dima, I. M., J. M. Wallace, and I. Kraucunas, 2005: Tropical zonal momentum balance in the NCEP reanalyses. *J. Atmos. Sci.*, **62**, 2499–2513, https://doi.org/10.1175/JAS3486.1.

Edman, J. P., and D. M. Romps, 2014: An improved weak pressure gradient scheme for single-column modeling. *J. Atmos. Sci.*, **71**, 2415–2429, https://doi.org/10.1175/JAS-D-13-0327.1.

Emanuel, K. A., 2019: Inferences from simple models of slow, convectively coupled processes. *J. Atmos. Sci.*, **76**, 195–208, https://doi.org/10.1175/JAS-D-18-0090.1.

——, J. D. Neelin, and C. S. Bretherton, 1994: On large-scale circulations in convecting atmospheres. *Quart. J. Roy. Meteor. Soc.*, **120**, 1111–1143, https://doi.org/10.1002/qj.49712051902.

Gill, A. E., 1980: Some simple solutions for heat-induced tropical circulation. *Quart. J. Roy. Meteor. Soc.*, **106**, 447–462, https://doi.org/10.1002/qj.49710644905.

Hawkins, H. F., and S. L. Rosenthal, 1965: On the computation of stream functions from the wind field. *Mon. Wea. Rev.*, **93**, 245–252, https://doi.org/10.1175/1520-0493(1965)093<0245:OTCOSF>2.3.CO;2.

Helfer, K. C., L. Nuijens, and V. V. Dixit, 2021: The role of shallow convection in the momentum budget of the trades from large-eddy-simulation hindcasts. *Quart. J. Roy. Meteor. Soc.*, **147**, 2490–2505, https://doi.org/10.1002/qj.4035.

Hersbach, H., and Coauthors, 2020: The ERA5 global reanalysis. *Quart. J. Roy. Meteor. Soc.*, **146**, 1999–2049, https://doi.org/10.1002/qj.3803.

Holloway, C. E., A. A. Wing, S. Bony, C. Muller, H. Masunaga, T. S. L'Ecuyer, D. D. Turner, and P. Zuidema, 2017: Observing convective aggregation. *Surv. Geophys.*, **38**, 1199–1236, https://doi.org/10.1007/s10712-017-9419-1.

Keil, P., H. Schmidt, B. Stevens, and J. Bao, 2021: Variations of tropical lapse rates in climate models and their implications for upper-tropospheric warming. *J. Climate*, **34**, 9747–9761, https://doi.org/10.1175/JCLI-D-21-0196.1.

Kuang, Z., 2008: Modeling the interaction between cumulus convection and linear gravity waves using a limited-domain cloud system-resolving model. *J. Atmos. Sci.*, **65**, 576–591, https://doi.org/10.1175/2007JAS2399.1.

Lin, J.-L., B. E. Mapes, and W. Han, 2008: What are the sources of mechanical damping in Matsuno–Gill-type models? *J. Climate*, **21**, 165–179, https://doi.org/10.1175/2007JCLI1546.1.

Lindzen, R. S., and S. Nigam, 1987: On the role of sea surface temperature gradients in forcing low-level winds and convergence in the tropics. *J. Atmos. Sci.*, **44**, 2418–2436, https://doi.org/10.1175/1520-0469(1987)044<2418:OTROSS>2.0.CO;2.

Manabe, S., and R. F. Strickler, 1964: Thermal equilibrium of the atmosphere with a convective adjustment. *J. Atmos. Sci.*, **21**, 361–385, https://doi.org/10.1175/1520-0469(1964)021<0361:TEOTAW>2.0.CO;2.

——, and R. T. Wetherald, 1967: Thermal equilibrium of the atmosphere with a given distribution of relative humidity. *J. Atmos. Sci.*, **24**, 241–259, https://doi.org/10.1175/1520-0469(1967)024<0241:TEOTAW>2.0.CO;2.

Mapes, B. E., 1993: Gregarious tropical convection. *J. Atmos. Sci.*, **50**, 2026–2037, https://doi.org/10.1175/1520-0469(1993)050<2026:GTC>2.0.CO;2.

Miller, R. L., 1997: Tropical thermostats and low cloud cover. *J. Climate*, **9**, 409–440, https://doi.org/10.1175/1520-0442(1997)010<0409:TTALCC>2.0.CO;2.

Nakajima, S., Y.-Y. Hayashi, and Y. Abe, 1992: A study on the "runaway greenhouse effect" with a one-dimensional radiative-convective equilibrium model. *J. Atmos. Sci.*, **49**, 2256–2266, https://doi.org/10.1175/1520-0469(1992)049<2256:ASOTGE>2.0.CO;2.

Neelin, J. D., and I. M. Held, 1987: Modeling tropical convergence based on the moist static energy budget. *Mon. Wea. Rev.*, **115**, 3–12, https://doi.org/10.1175/1520-0493(1987)115<0003:MTCBOT>2.0.CO;2.

Pierrehumbert, R. T., 1995: Thermostats, radiator fins, and the local runaway greenhouse. *J. Atmos. Sci.*, **52**, 1784–1806, https://doi.org/10.1175/1520-0469(1995)052<1784:TRFATL>2.0.CO;2.

Raymond, D. J., 1992: Nonlinear balance and potential-vorticity thinking at large Rossby number. *Quart. J. Roy. Meteor. Soc.*, **118**, 987–1015, https://doi.org/10.1002/qj.49711850708.

——, Ž. Fuchs, S. Gjorgjievska, and S. Sessions, 2015: Balanced dynamics and convection in the tropical troposphere. *J. Adv. Model. Earth Syst.*, **7**, 1093–1116, https://doi.org/10.1002/2015MS000467.

Romps, D. M., 2012: Weak pressure gradient approximation and its analytical solutions. *J. Atmos. Sci.*, **69**, 2835–2845, https://doi.org/10.1175/JAS-D-11-0336.1.

Sangster, W. E., 1987: An improved technique for computing the horizontal pressure-gradient force at the Earth's surface. *Mon. Wea. Rev.*, **115**, 1358–1369, https://doi.org/10.1175/1520-0493(1987)115<1358:AITFCT>2.0.CO;2.

Sarachik, E. S., 1978: Tropical sea surface temperature: An interactive one-dimensional atmosphere-ocean model. *Dyn. Atmos. Oceans*, **2**, 455–469, https://doi.org/10.1016/0377-0265(78)90014-3.

Sardeshmukh, P. D., and B. J. Hoskins, 1988: The generation of global rotational flow by steady idealized tropical divergence. *J. Atmos. Sci.*, **45**, 1228–1251, https://doi.org/10.1175/1520-0469(1988)045<1228:TGOGRF>2.0.CO;2.

Schwendike, J., P. Govekar, M. J. Reeder, R. Wardle, G. J. Berry, and C. Jakob, 2014: Local partitioning of the overturning circulation in the tropics and the connection to the Hadley and Walker circulations. *J. Geophys. Res. Atmos.*, **119**, 1322–1339, https://doi.org/10.1002/2013JD020742.

Sessions, S. L., S. Sugaya, D. J. Raymond, and A. H. Sobel, 2010: Multiple equilibria in a cloud-resolving model using the weak temperature gradient approximation. *J. Geophys. Res.*, **115**, D12110, https://doi.org/10.1029/2009JD013376.

Sherwood, S. C., 1999: Feedbacks in a simple prognostic tropical climate model. *J. Atmos. Sci.*, **56**, 2178–2200, https://doi.org/10.1175/1520-0469(1999)056<2178:FIASPT>2.0.CO;2.

Singh, M. S., and P. A. O'Gorman, 2013: Influence of entrainment on the thermal stratification in simulations of radiative-convective equilibrium. *Geophys. Res. Lett.*, **40**, 4398–4403, https://doi.org/10.1002/grl.50796.

——, and ——, 2015: Increases in moist-convective updraught velocities with warming in radiative-convective equilibrium. *Quart. J. Roy. Meteor. Soc.*, **141**, 2828–2838, https://doi.org/10.1002/qj.2567.

Sobel, A. H., 2002: Water vapor as an active scalar in tropical atmospheric dynamics. *Chaos*, **12**, 451–459, https://doi.org/10.1063/1.1480795.

——, and C. S. Bretherton, 2000: Modeling tropical precipitation in a single column. *J. Climate*, **13**, 4378–4392, https://doi.org/10.1175/1520-0442(2000)013<4378:MTPIAS>2.0.CO;2.

Stevens, B., and Coauthors, 2019: Dyamond: The dynamics of the atmospheric general circulation modeled on non-hydrostatic domains. *Prog. Earth Planet. Sci.*, **6**, 61, https://doi.org/10.1186/s40645-019-0304-z.

Van Tuyl, A. H., 1986: Advective influences on forced tropical motions. *J. Atmos. Sci.*, **43**, 141–161, https://doi.org/10.1175/1520-0469(1986)043<0141:AIOFTM>2.0.CO;2.

Wang, S., and A. H. Sobel, 2011: Response of convection to relative sea surface temperature: Cloud-resolving simulations in two and three dimensions. *J. Geophys. Res.*, **116**, D11119, https://doi.org/10.1029/2010JD015347.

Warren, R. A., M. S. Singh, and C. Jakob, 2020: Simulations of radiative-convective-dynamical equilibrium. *J. Adv. Model. Earth Syst.*, **12**, e2019MS001734, https://doi.org/10.1029/2019MS001734.

Wing, A. A., K. Emanuel, C. E. Holloway, and C. Muller, 2018a: Convective self-aggregation in numerical simulations: A review. *Shallow Clouds, Water Vapor, Circulation, and Climate Sensitivity*, R. Pincus et al., Eds., Space Sciences Series of ISSI, Vol. 65, Springer Publishing, 1–25, https://doi.org/10.1007/978-3-319-77273-8_1.

——, K. A. Reed, M. Satoh, B. Stevens, S. Bony, and T. Ohno, 2018b: Radiative–convective equilibrium model intercomparison project. *Geosci. Model Dev.*, **11**, 793–813, https://doi.org/10.5194/gmd-11-793-2018.

Wu, G., B. He, Y. Liu, Q. Bao, and R. Ren, 2015: Location and variation of the summertime upper-troposphere temperature maximum over South Asia. *Climate Dyn.*, **45**, 2757–2774, https://doi.org/10.1007/s00382-015-2506-4.

Xu, K.-M., and K. A. Emanuel, 1989: Is the tropical atmosphere conditionally unstable? *Mon. Wea. Rev.*, **117**, 1471–1479, https://doi.org/10.1175/1520-0493(1989)117<1471:ITTACU>2.0.CO;2.

Yang, D., and S. D. Seidel, 2020: The incredible lightness of water vapor. *J. Climate*, **33**, 2841–2851, https://doi.org/10.1175/JCLI-D-19-0260.1.

Yang, W., R. Seager, and M. A. Cane, 2013: Zonal momentum balance in the tropical atmospheric circulation during the global monsoon mature months. *J. Atmos. Sci.*, **70**, 583–599, https://doi.org/10.1175/JAS-D-12-0140.1.

Yasunaga, K., and B. Mapes, 2012: Differences between more divergent and more rotational types of convectively coupled equatorial waves. Part I: Space–time spectral analyses. *J. Atmos. Sci.*, **69**, 3–16, https://doi.org/10.1175/JAS-D-11-033.1.

Zhang, Y., and S. Fueglistaler, 2020: How tropical convection couples high moist static energy over land and ocean. *Geophys. Res. Lett.*, **47**, e2019GL086387, https://doi.org/10.1029/2019GL086387.

Zhou, W., and S.-P. Xie, 2019: A conceptual spectral plume model for understanding tropical temperature profile and convective updraft velocities. *J. Atmos. Sci.*, **76**, 2801–2814, https://doi.org/10.1175/JAS-D-18-0330.1.